Supplementary Information for:

Electrochemical Biomass Valorization on Gold-Metal Oxide Nanoscale Heterojunctions Enables Investigation of both Catalyst and Reaction Dynamics with *Operando* Surface-Enhanced Raman Spectroscopy

Nina Heidary[1] and Nikolay Kornienko[1*]

[1]Department of Chemistry, Université de Montréal, Roger-Gaudry Building, Montreal, Quebec H3C 3J7, Canada.

*Email: Nikolay.kornienko@umontreal.ca

Catalyst Synthesis: Au dendrites were deposited through a two-step deposition process. A first layer of Au was deposited from a 160 mM $KAuCl_4$ solution (0.5M HCl) electrolyte at -0.4V vs. Ag/AgCl for 3 minutes. Then the process was repeated on the same electrode with a 20 mM $KAuCl_4$ solution (0.5M HCl) electrolyte at -0.4V vs. Ag/AgCl for 1 minute. After rinsing copiously with Milli-Q water, a think Zn layer was deposited through electrodeposition in 1 mM $ZnNO_3$ in 0.1M pH7 potassium phosphate buffer for 2 minutes at -1.2 V vs. Ag/AgCl. After rinsing with Milli-Q water again, the Zn was replaced with the transition metal of choice by soaking for 15 minutes in a 1.0M solution of the nickel acetate, iron chloride, or cobalt chloride. Mixed-metal films were generated by soaking in 0.5M solution of two metals (Ni and Fe or Co and Fe).

Electrocatalysis: Electrochemical experiments were conducted in two-compartment, custom built glass cells separated with a porous glass frit. Ag/AgCl reference electrodes and graphitic carbon rod counter electrodes were used. As an Hg/HgO reference was difficult to obtain due to university restrictions and Ag/AgCl is not always stable for long durations ref in alkaline electrolyte, the used Ag/AgCl reference was periodically checked against a master reference electrode for any potential drifts over time. A biologic VMP200 potentiostat and EC-lab software were employed for electrochemical experiments. The IR drop was compensated for at 85% with the software's ZIR program by first recording the impedance between the working and reference electrode at open circuit at 100 KHz frequency. Typically, 10- or 15-mL reaction volume was used. Reaction products were quantified with NMF using an acetate internal standard.

Raman Spectroscopy: Raman spectroscopy was performed with a Renishaw Invia system. For both *operando* and ex-situ measurements, a 633 nm laser was employed. The line focus configuratioj was applied with the Renishaw, which spread the laser beam out over the sample to avoid sample damage. A Zeiss 40X water immersion objective was used for *Operando* measurements, which were conducted in a home-built electrochemical cell constructed from Teflon. Typical acquisition times were 20-30 seconds. Spectra were first acquired at the most negative voltage and the voltage was progressively increased in a chronoamerometric scan. Cosmic ray removal was applied during the spectroscopic experiment. Spectra were not smoothed or background-corrected to avoid losing any spectral information in the process.

Electron Microscopy: Electron microscopy was performed at the Centre for Characterization and Mircoscopy of Materials at Polytechnique Montreal. SEM images were acquired on the samples post synthesis and for TEM imaging, the catalysts were simply scratched off onto ultrathin carbon/copper TEM grids.

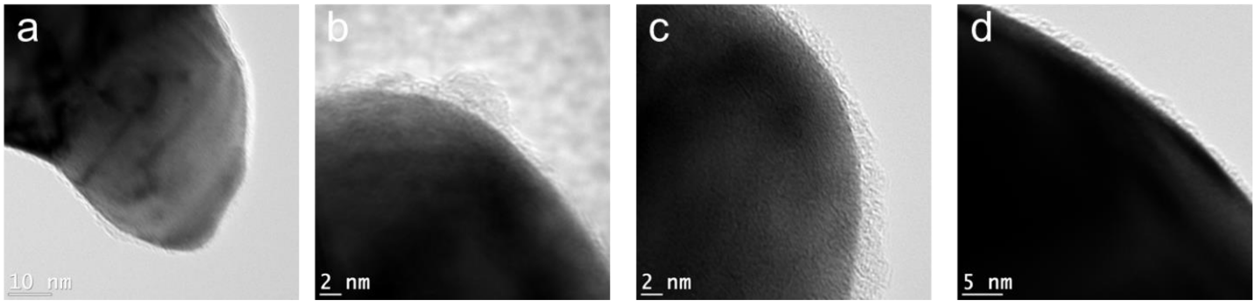

Figure S1: Additional representative TEM images of AuNi catalysts (a-d).

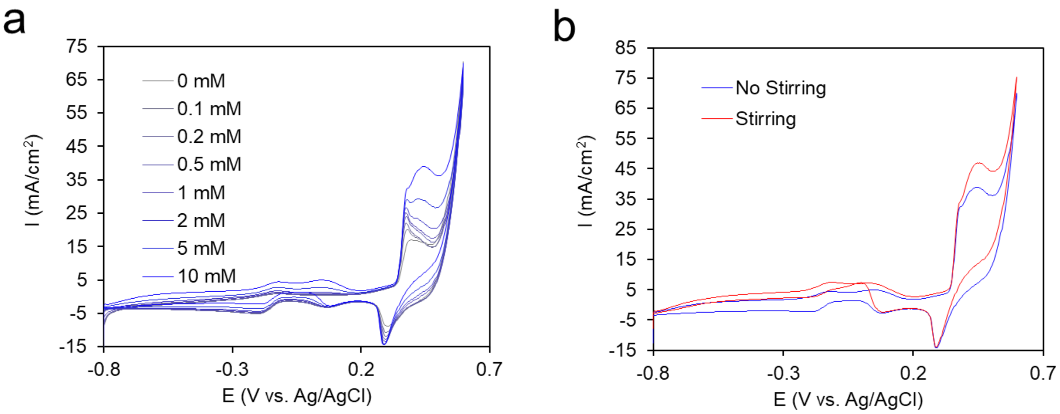

Figure S2: CVs with successively increasing HMF concentrations (1M KOH) for AuNi (a), and a CV with stirring of the solution at 1600 rpm vs. without (b).

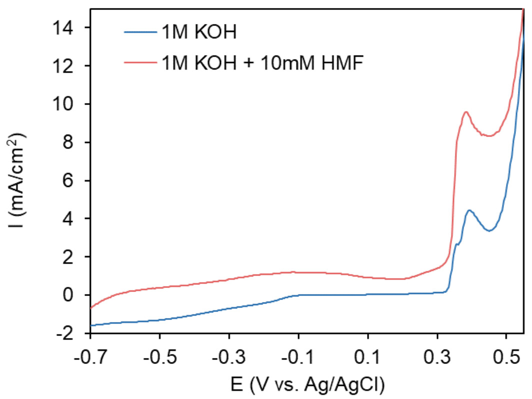

Figure S3: Slow linear scan at 1mV/s of AuNi with and without HMF in the solution.

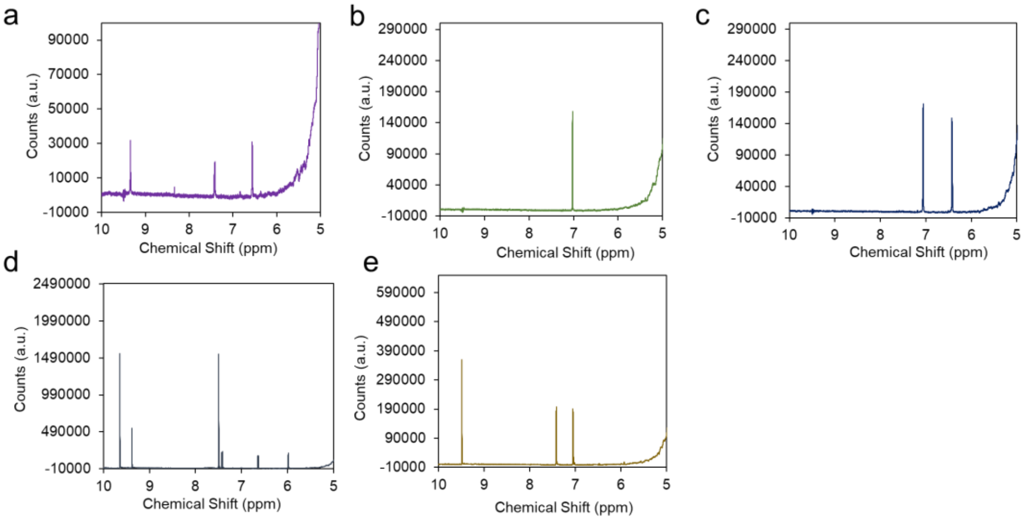

Figure S4: NMR spectra of HMF (a), FDCA (b), HMFCA (c), DFF (d) and FFCA in 10mM KOH.

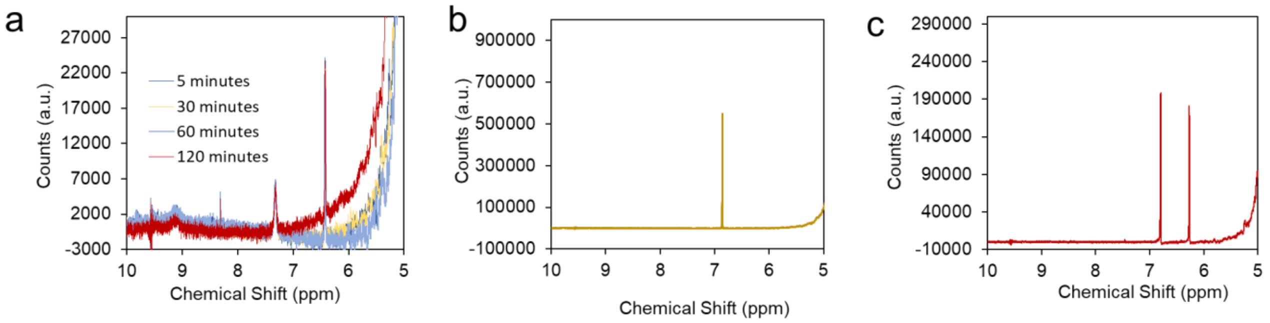

Figure S5: NMR spectra of HMF (a), FDCA (b), and HMFCA (c) in 1M KOH. A decomposition product of HMF begins to build up at 8.5 ppm in small quantities, though it is more prevalent in the catalytic runs that take place >24 hrs in which the HMF is not fully converted.

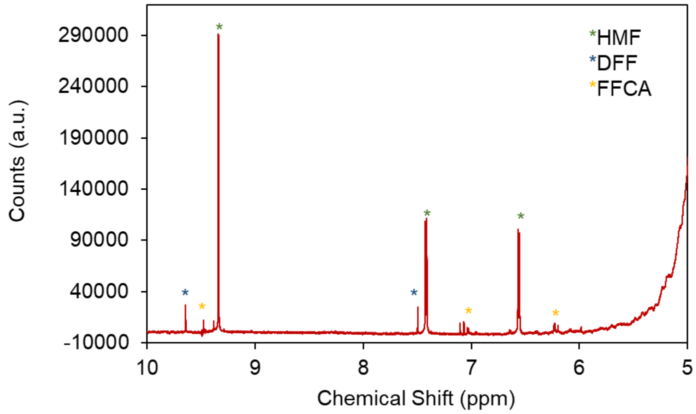

Figure S6: NMR spectrum of HMF oxidized at 1.2V on AuNi in 10mM KOH after 24 hrs of electrolysis. The faradaic efficiencies for DFF and FFCA we 12% and 10%, respectively, with the remainder of the current presumably going towards water oxidation.

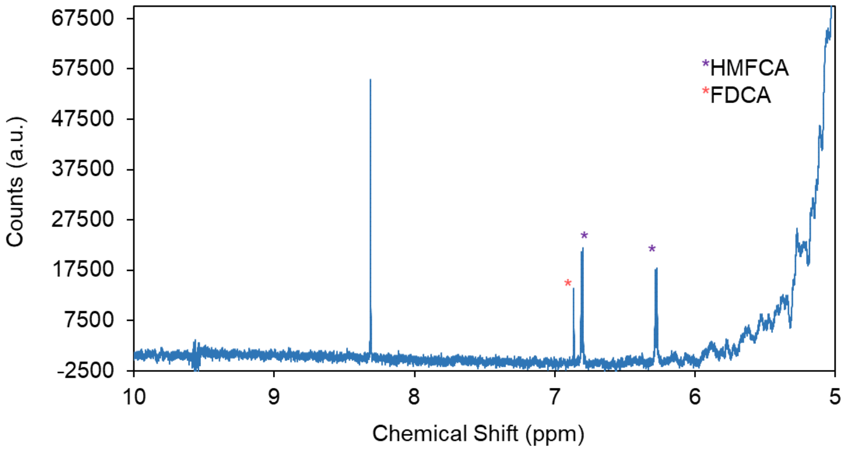

Figure S7: NMR spectrum of HMF oxidized at 0.1V on AuNi in 1M KOH after 24 hrs of electrolysis. HMFCA and FDCA were formed with 35% and 40% Faradaic efficiency, respectively.

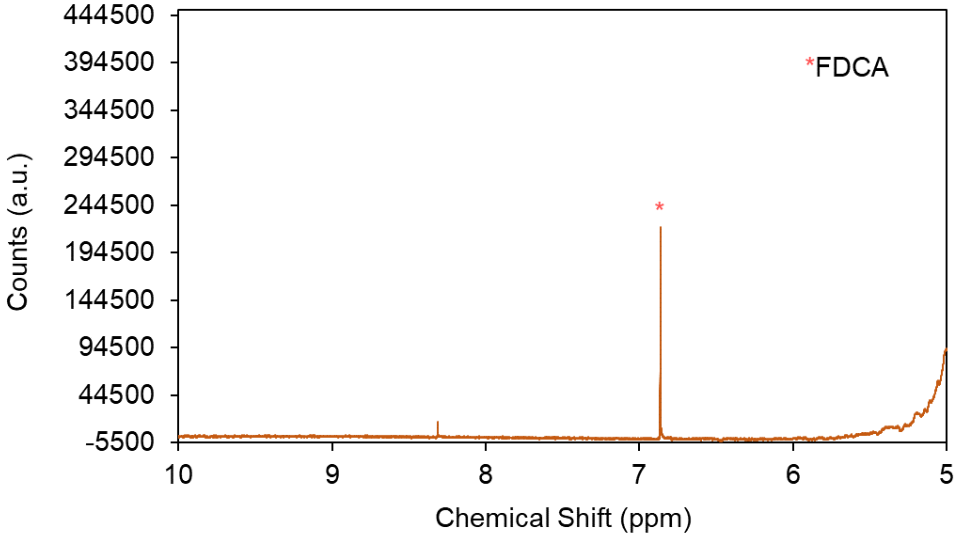

Figure S8: NMR spectrum of HMF oxidized at 0.4V on AuNi in 1M KOH after 5 hrs of electrolysis. FDCA was formed with approximately 99% Faradaic efficiency.

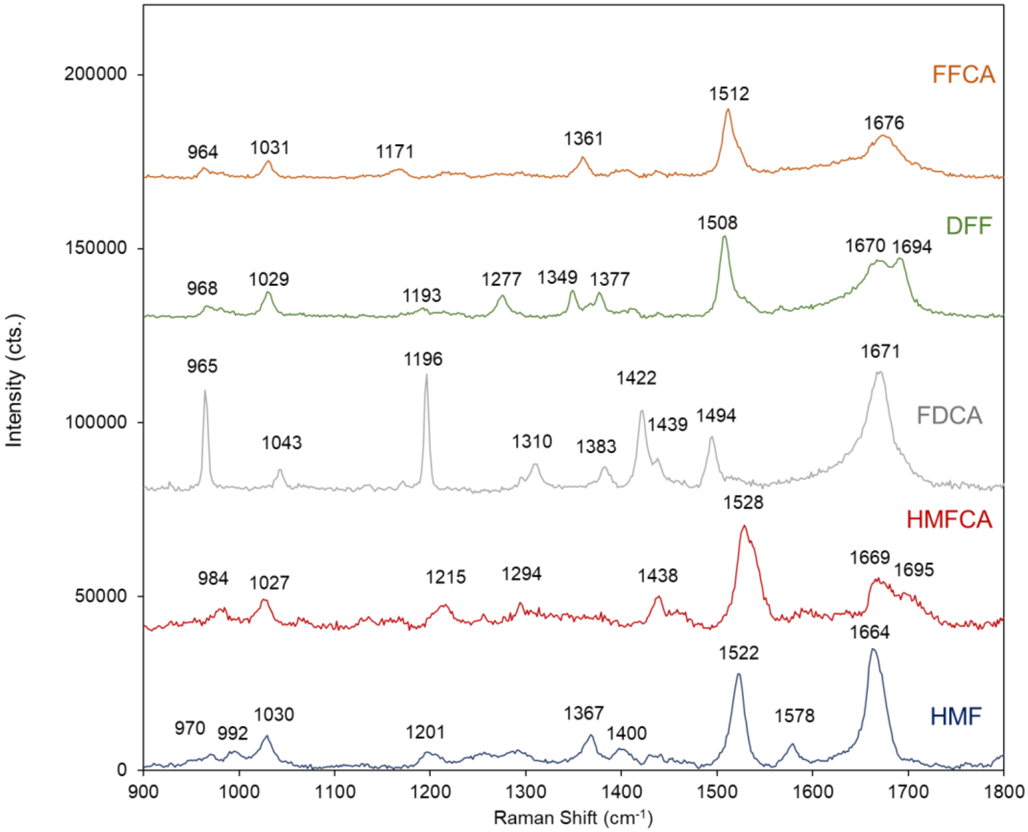

Figure S9: Raman spectra of solutions of HMF and potential products in 10mM KOH.

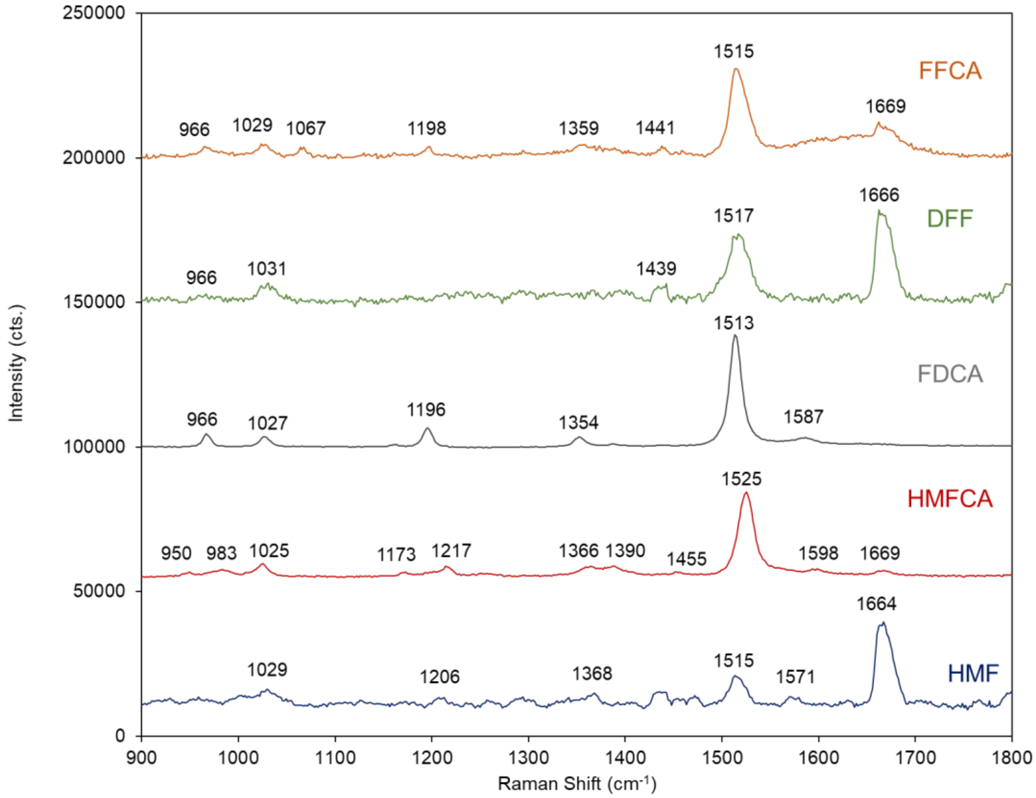

Figure S10: Raman spectra of solutions of HMF and potential products in 1M KOH.

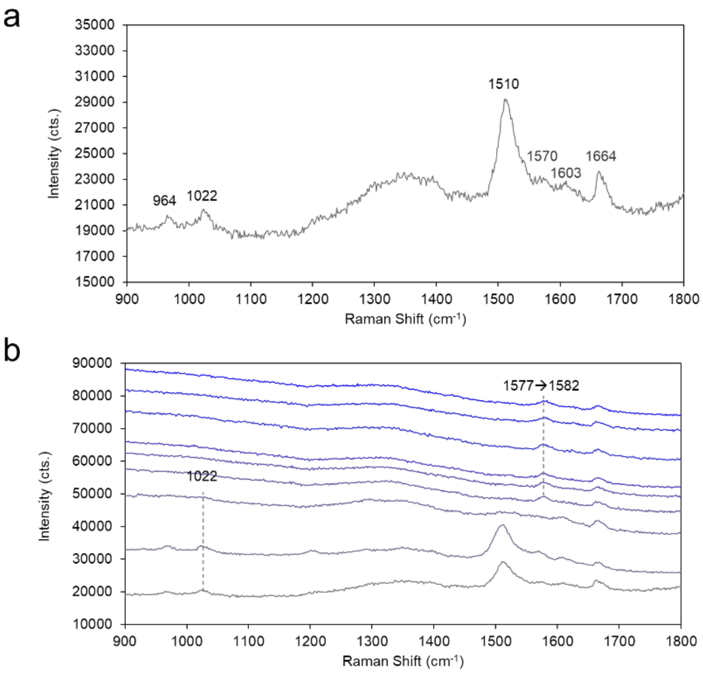

Figure S11: Raman spectrum of HMF on AuNi in 10mM KOH at open circuit (a). Broad bands around 1350 and 1600 cm^{-1} stem from the carbon paper substrate. The 1022 cm^{-1} band disappears as the 1577 cm^{-1} band emerges (b).

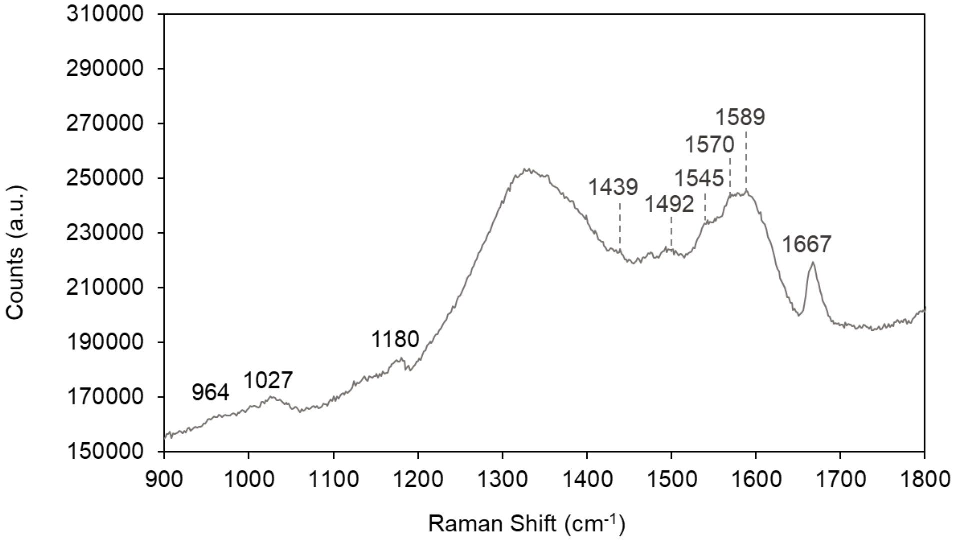

Figure S12: Raman spectrum of HMF on AuNi in 1M KOH at open circuit. Broad bands around 1350 and 1600 cm^{-1} stem from the carbon paper substrate.

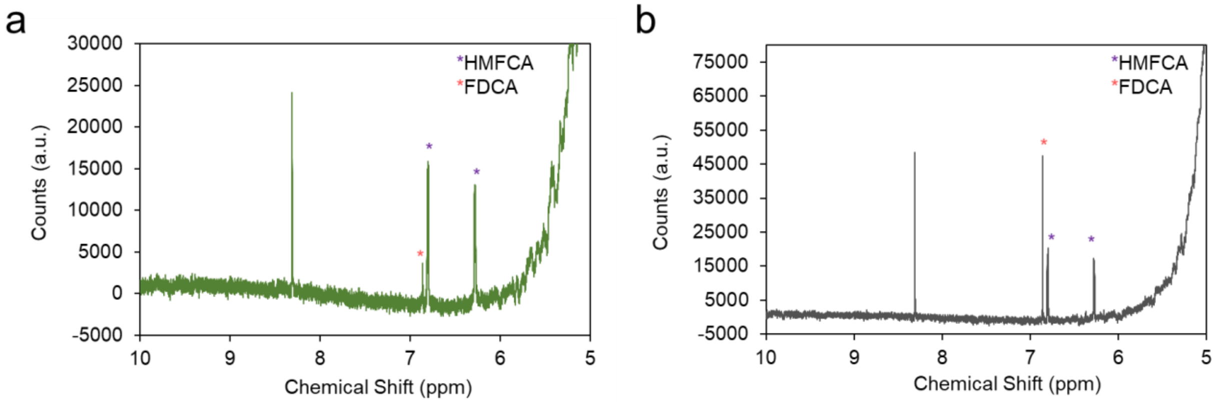

Figure S13: NMR spectra of the reaction solution after electrolysis with AuCo at 0.25V for 24 hrs (a) and 0.4V for 24 hrs (b) in 1M KOH. The Faradaic efficiencies for HMFCA and FDCA were in 55%(HMFCA) and 23% (FDCA) in (a). The Faradaic efficiencies for HMFCA and FDCA were 28%(HMFCA) and 50%(FDCA) in (b).

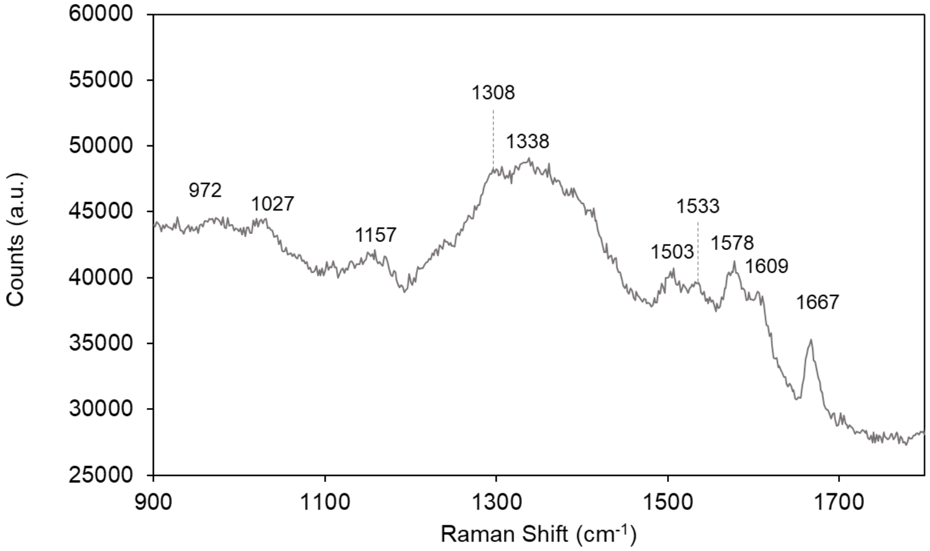

Figure S14: Raman spectrum of HMF on AuCo in 1M KOH under open circuit conditions. Broad bands around 1350 and 1600 cm^{-1} stem from the carbon paper substrate.

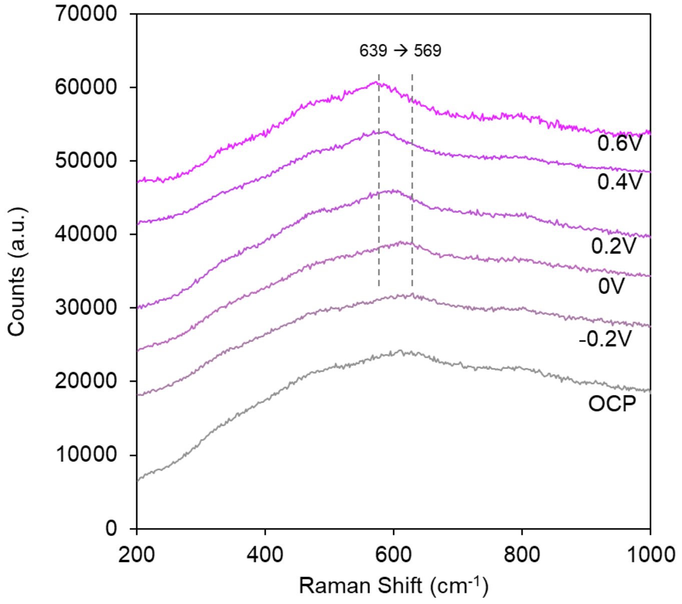

Figure S15: Raman spectra of AuCo in 1MKOH in the absence of HMF in the solution.

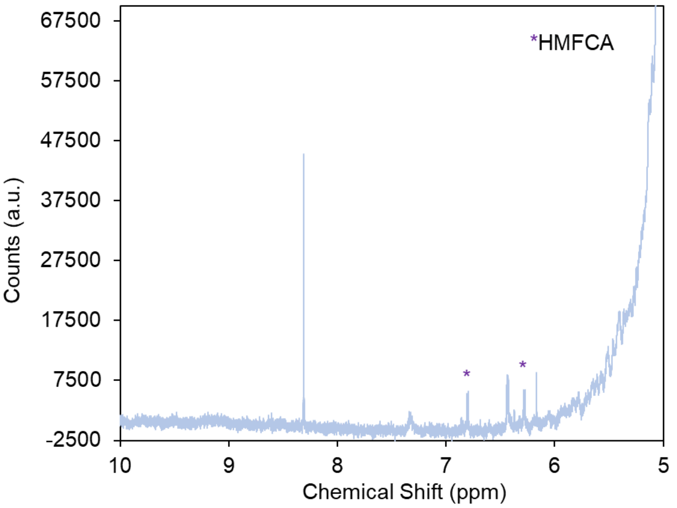

Figure S16: NMR spectrum of the reaction solution after electrolysis with Au at 0.4V in 1M KOH. HMFCA was formed with 24% Faradaic efficiency.

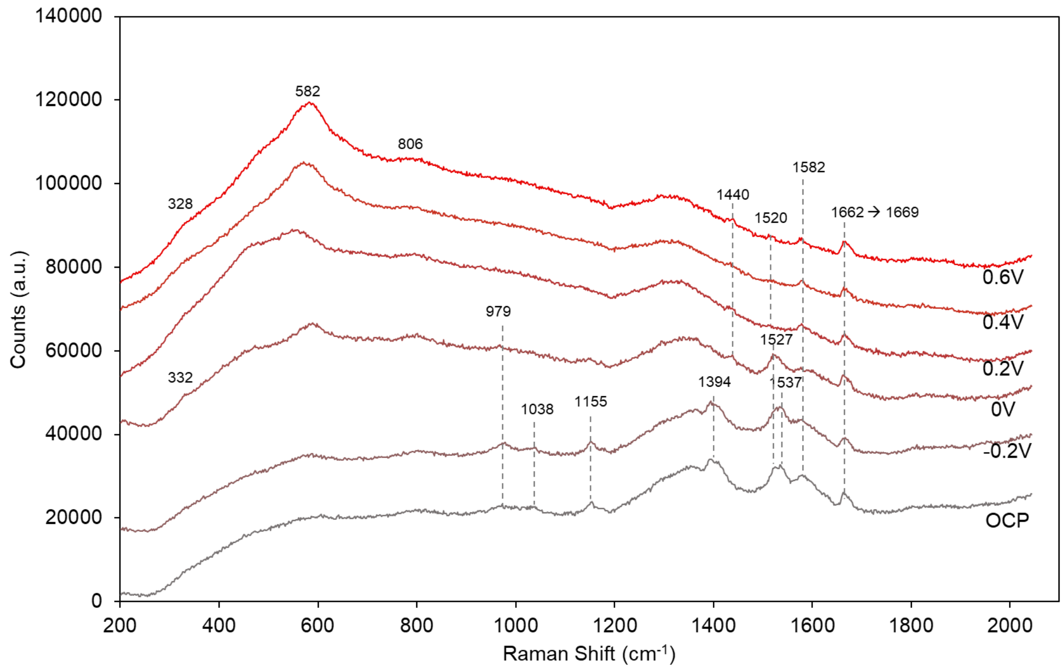

Figure S17: Raman spectra of Au in 1M KOH with 10 mM HMF as a function of applied potential.

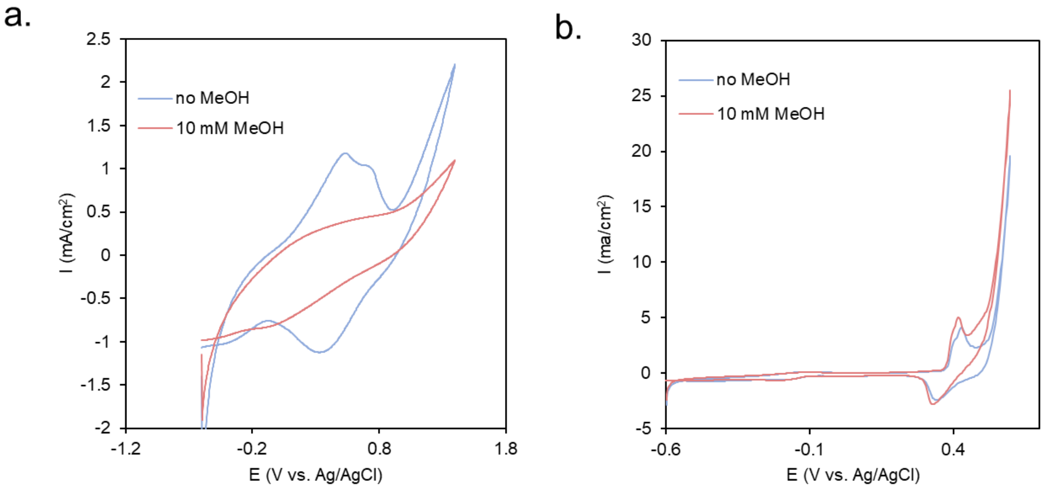

Figure S18: CVs of AuNi catalysts in the presence and absence of methanol in 10mM KOH (a) and 1M KOH (b).

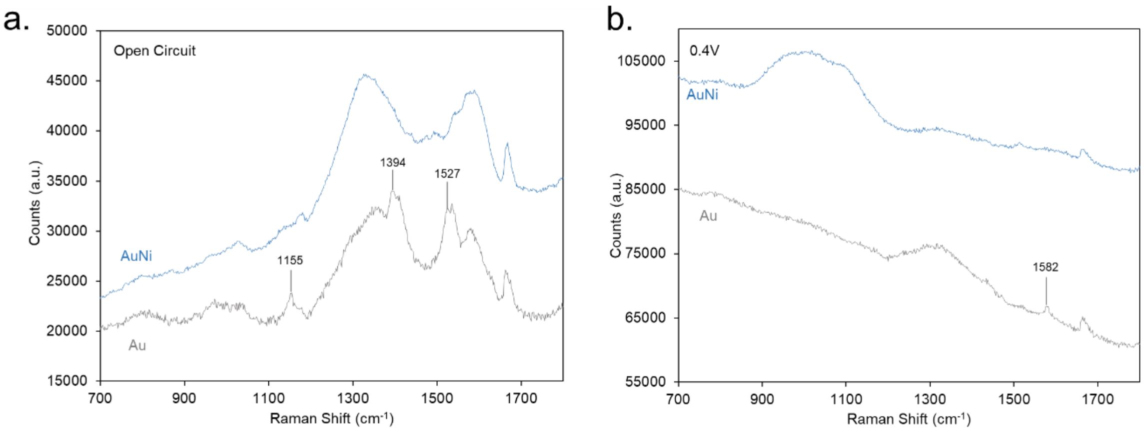

Figure S19: Comparison of the Raman spectra in 1M KOH with 10mM HMF of Au and AuNi catalysts at open circuit (a) and 0.4V (b). Several distinct spectral features are noted on the Au catalysts only and their lack in the AuNi spectra indicates, for the most part, a lack of exposed underlying Au.